Available online at www.sciencedirect.com

ScienceDirect

Procedia Structural Integrity 28 (2020) 418–429

Structural Integrity Procedia

www.elsevier.com/locate/procedia

1st Virtual European Conference on Fracture

Effect of horizon shape in peridynamics

Selda Oterkus[a,*], Bingquan Wang[a], Erkan Oterkus[a]

[a]PeriDynamics Research Centre, Department of Naval Architecture, Ocean and Marine Engineering, University of Strathclyde, 100 Montrose Street, Glasgow G4 0LZ, UK

Abstract

As a new continuum mechanics formulation, peridynamics has a non-local character by having an internal length scale parameter called horizon. Although the effect of the size of the horizon has been studied earlier, the shape of the horizon can also be influential. In this study, the effect of horizon shape is investigated for both ordinary state-based and non-ordinary state-based peridynamics. Three different horizon shapes are considered including circle, irregular and square. Both static and dynamic analyses are studied by considering plate under tension and vibration of a plate problems. For both static and dynamic conditions, square shape could not capture accurate vertical displacements for ordinary-state based peridynamics. On the other hand, results obtained for all three horizon shapes agree very well with finite element analysis results for non-ordinary state-based peridynamics.

Keywords: Peridynamics; Horizon; Shape; Non-local

1. Introduction

Classical continuum mechanics which is widely used in solid mechanics is facing difficulties for predicting crack propagation since its equations contain spatial derivatives of displacements and such derivatives are not defined along crack surfaces. To overcome this problem, a new continuum mechanics formulation, peridynamics (PD), was developed by Silling (2000) using integro-differential equations without spatial derivatives. Since then PD has been

* Corresponding author. Tel.: +44-141-548-3876.
E-mail address: selda.oterkus@strath.ac.uk

2452-3216
10.1016/j.prostr.2020.10.049

utilized for the analysis of various challenging problems. Amongst these Imachi et. al. (2019) developed new transition bond concept and then applied it for crack arrest in Imachi et. al. (2020). Liu et. al. (2018) used peridynamics at nano-scale and analyzed fracture behavior of zigzag graphene sheets. Oterkus et. al. (2010a) utilized peridynamics for damage analysis of bolted joint of composite structures based on the formulation presented in Oterkus and Madenci (2012a,b). PD has also been used for meso-scale analysis by De Meo et. al. (2016) and Zhu et. al. (2016) to predict fracture in polycrystalline materials. Moreover, Vazic et. al. (2017) and Basoglu et. al. (2019) investigated interactions between micro-cracks and macro-cracks. An interesting application of peridynamics is topology optimization of cracked structures which was presented by Kefal et. al. (2019). PD is also suitable for impact analysis such as the impact analysis of reinforced concrete considered by Oterkus et. al. (2012). Fatigue analysis is also possible in PD framework as shown in Oterkus et. al. (2010b). Simplified structures such as beams, plates and shells can also be represented by using peridynamics. Euler-Bernoulli beam formulation was developed by Diyaroglu et al. (2019) which was further extended to Kirchhoff plate formulation by Yang et. al. (2020). For Winkler foundations, Vazic et. al. (2020) introduced a model for Mindlin plates resting on Winkler foundations. Although PD formulations and classical finite element formulations have fundamental differences, PD formulations can be implemented in commercial finite element software packages as explained in Yang et. al. (2019). Peridynamics is not limited to mechanical analysis and can be used for the analysis of other fields. For instance, Diyaroglu et. al. (2017a) presented peridynamic diffusion formulation. Moisture is an important concern for the durability of electronic packages. Therefore, Oterkus et. al. (2014) and Diyaroglu et. al. (2017b) used PD for moisture analysis of electronic packages. Wang et. al. (2018) investigated the fracture evolution in lithiation process for electrodes of Lithium-Ion batteries. Corrosion can also be modelled by using peridynamics. De Meo et. al. (2017) investigated crack evolution starting from corrosion pit areas by using the formulation presented in De Meo and Oterkus (2017).

Another important difference between peridynamics and classical continuum formulation is the length scale parameter of peridynamics, horizon, which doesn't exist in classical formulation. Horizon defines the range of non-local peridynamic interactions. The size of the horizon has been investigated in various studies including Silling and Askari (2005), Bobaru and Hu (2012) and Wang et. al. (2020). However, the shape of the horizon can also be important and circular or spherical shape horizons are widely used. In this study, the effect of the shape of peridynamic horizon is investigated by considering various horizon shapes including circle, irregular and square for ordinary state-based and non-ordinary state-based peridynamic formulations under static and dynamic conditions.

2. Peridynamic theory

2.1. Ordinary state-based peridynamics

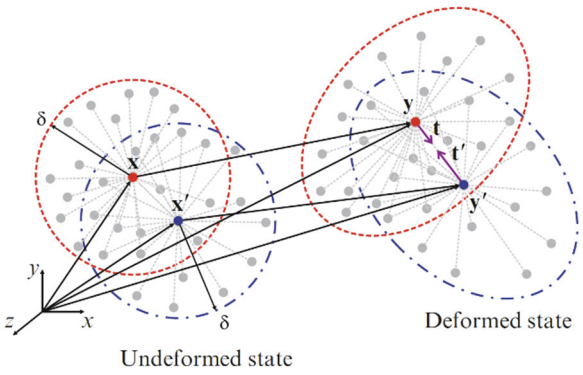

Fig. 1. Peridynamic forces in ordinary state-based peridynamics (Madenci and Oterkus, 2014).

Peridyamics is a new continuum mechanics formulation. A material point can interact with other material points inside its influence domain, horizon, in a non-local manner as shown in Fig. 1. According to ordinary state-based peridynamics, it is assumed that peridynamic forces between interacting material points are along the interaction direction but with different magnitudes. Moreover, the peridynamic forces are not only depending on the motion of interacting material points but also motion of material points inside their horizons. The equations of motion in ordinary state-based peridynamics can be written as (Madenci and Oterkus, 2014)

$$\rho(\mathbf{x})\ddot{\mathbf{u}}(\mathbf{x},t)=\int_{H_{\mathbf{x}}}\left(\mathbf{t}-\mathbf{t}'\right)dV'+\mathbf{b}(\mathbf{x},t) \tag{1}$$

where ρ is density, $\ddot{\mathbf{u}}$ is acceleration, $H_{\mathbf{x}}$ is the horizon and $\mathbf{b}$ is the body load vector. In Eq. (1) $\mathbf{t}$ and $\mathbf{t}'$ represent the peridynamic forces that the material points $\mathbf{x}$ and $\mathbf{x}'$ exert on each other which are defined as

$$\mathbf{t}=\left(\frac{2ad\delta}{|\mathbf{x}'-\mathbf{x}|}\theta(\mathbf{x},t)+b\,s\right)\frac{\mathbf{y}'-\mathbf{y}}{|\mathbf{y}'-\mathbf{y}|} \tag{2a}$$

$$\mathbf{t}'=\left(\frac{2ad\delta}{|\mathbf{x}'-\mathbf{x}|}\theta(\mathbf{x}',t)+b\,s\right)\frac{\mathbf{y}-\mathbf{y}'}{|\mathbf{y}-\mathbf{y}'|} \tag{2b}$$

where $\mathbf{y}$ and $\mathbf{y}'$ are the position of the material points $\mathbf{x}$ and $\mathbf{x}'$ in the deformed configuration, respectively, δ is the horizon size, and s is the stretch which is defined as

$$s=\frac{|\mathbf{y}'-\mathbf{y}|-|\mathbf{x}'-\mathbf{x}|}{|\mathbf{x}'-\mathbf{x}|} \tag{3}$$

a, b and d are peridynamic parameters which can be expressed for 2-dimensional problems as

$$a=\frac{E(3\nu-1)}{4(1-\nu^2)} \tag{4a}$$

$$b=\frac{3E}{\pi h\delta^4(1+\nu)} \tag{4b}$$

$$d=\frac{2}{\pi h\delta^3} \tag{4c}$$

where E and ν are elastic modulus and Poisson's ratio, respectively, and h is the thickness. The peridynamic dilatation, θ is defined as

$$\theta(\mathbf{x},t)=\int_{H_{\mathbf{x}}}(d\,\delta s)\,dV' \tag{5}$$

2.2. Non-ordinary state-based peridynamics

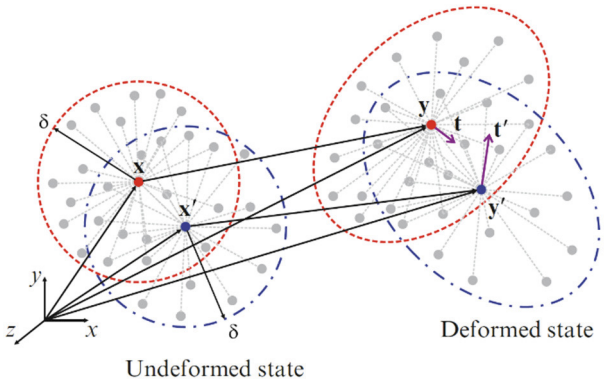

Fig. 2. Peridynamic forces in non-ordinary state-based peridynamics (Madenci and Oterkus, 2014).

As mentioned in the previous section, an assumption is made in ordinary state-based peridynamics regarding the direction of peridynamic forces being along the interaction direction. For non-ordinary state-based peridynamics, this assumption is relaxed so that interaction forces can be in arbitrary directions. Moreover, non-ordinary state based peridynamics is a suitable platform to incorporate classical material models in peridynamic framework. Peridynamic forces that the material points $\mathbf{x}$ and $\mathbf{x}'$ exert on each other in non-ordinary state-based peridynamics can be written as

$$\mathbf{t}=\omega\mathbf{P}[\mathbf{x}]\mathbf{K}^{-1}[\mathbf{x}](\mathbf{x}'-\mathbf{x}) \tag{6a}$$

$$\mathbf{t}'=\omega\mathbf{P}[\mathbf{x}']\mathbf{K}^{-1}[\mathbf{x}'](\mathbf{x}-\mathbf{x}') \tag{6b}$$

where ω is the influence function, $\mathbf{P}[\mathbf{x}]$ is the first Piola-Kirchhoff tensor of the material point $\mathbf{x}$, and $\mathbf{K}[\mathbf{x}]$ is the tensor of the material point $\mathbf{x}$ which is defined as

$$\mathbf{K}[\mathbf{x}]=\int_{H_{\mathbf{x}}}\omega\big((\mathbf{x}'-\mathbf{x})\otimes(\mathbf{x}'-\mathbf{x})\big)\,dV' \tag{7}$$

with the symbol " $\otimes$ " being the dyadic product. To calculate the first-Piola Kirchhoff tensor in peridynamic framework, it is essential to define the deformation tensor in peridynamic framework, $\tilde{\mathbf{F}}[\mathbf{x}]$ which can be written as

$$\tilde{\mathbf{F}}[\mathbf{x}] = \frac{\int_{H_x} \omega\left((\mathbf{y}'-\mathbf{y})\otimes(\mathbf{x}'-\mathbf{x})\right)dV'}{\int_{H_x} \omega\left((\mathbf{x}'-\mathbf{x})\otimes(\mathbf{x}'-\mathbf{x})\right)dV'} \tag{8}$$

The original non-ordinary state-based peridynamics suffer from zero-energy mode problem. To overcome this problem, Silling (2017) introduced an additional stability term to peridynamic forces given in Eqs. (6a,b) as

$$\mathbf{t} = \omega\left(\mathbf{P}[\mathbf{x}]\mathbf{K}^{-1}[\mathbf{x}](\mathbf{x}'-\mathbf{x}) + \frac{Gc}{w_0\delta}\mathbf{z}\right) \tag{9}$$

with

$$w_0 = \int_{H_x} \omega\, dV' \tag{10}$$

and

$$\mathbf{z} = (\mathbf{y}'-\mathbf{y}) - \tilde{\mathbf{F}}(\mathbf{x}'-\mathbf{x}) \tag{11}$$

In Eq. (9), G is a positive constant and c is the bond constant.

3. Numerical results

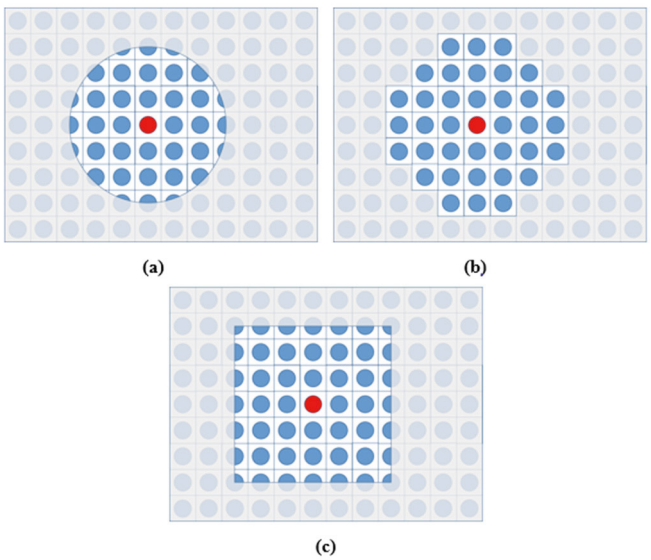

Fig. 3. Horizon shapes considered in this study, (a) circle, (b) irregular, (c) square.

To investigate the effect of horizon shape, three different horizon shapes were considered including circular, irregular and square shapes as shown in Fig. 3. Both static and dynamic analysis cases were studied for plate under tension and vibration of a plate problems.

3.1. Plate under tension

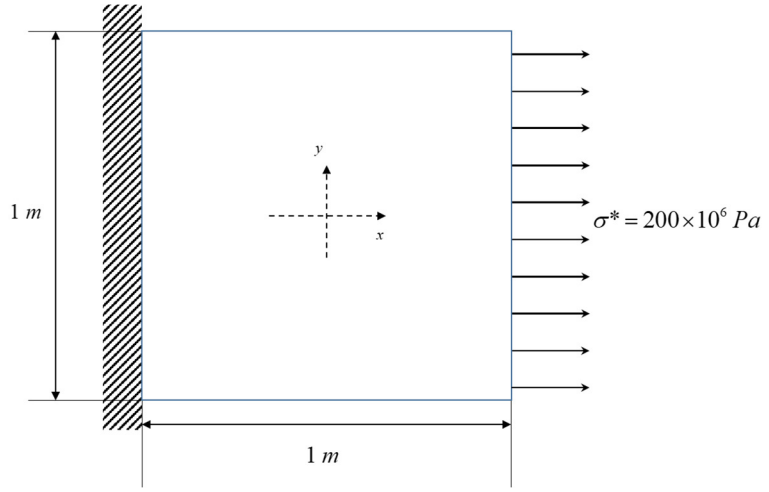

Fig. 4. Square plate subjected to tension loading.

In the first problem case, a square plate subjected to tension loading was considered as shown in Fig. 4. The square plate has a 1m edge length and thickness of 0.01 m. The elastic modulus and Poisson's ratio were specified as 200 GPa and 1/3, respectively. A uni-axial loading condition of $\sigma^* = 200\times10^6$ Pa in the *x*-direction at the right edge was applied whereas the left edge is fully fixed.

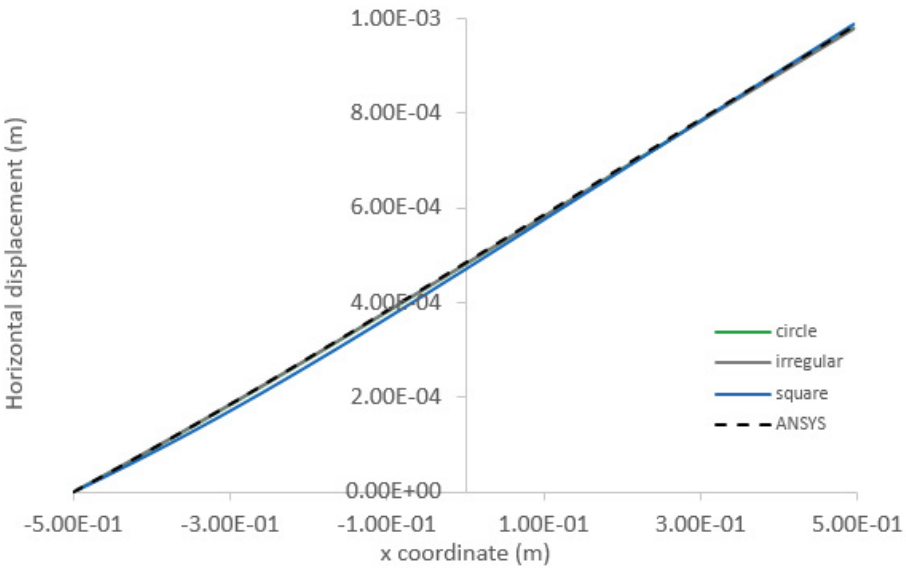

(a)

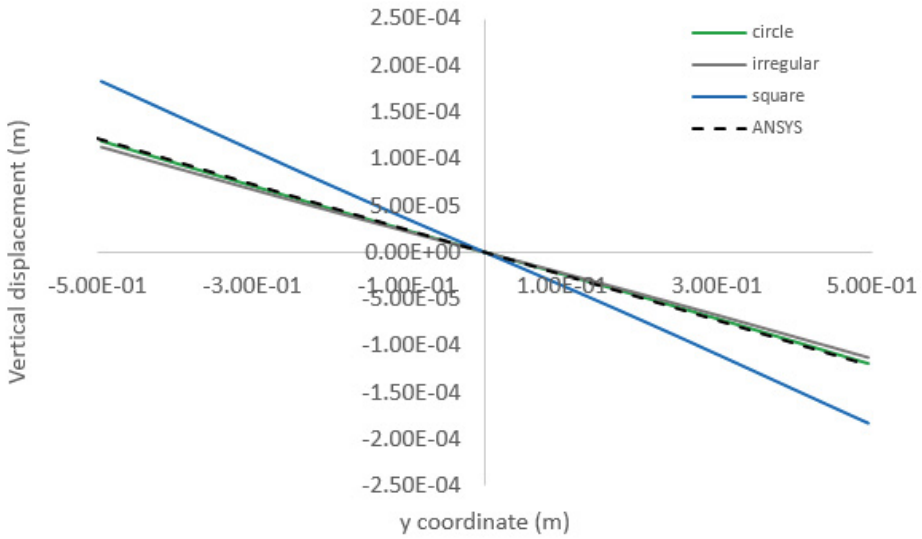

(b)

Fig. 5. Variation of **(a)** horizontal displacements along the central *x*-axis and **(b)** vertical displacements along the central y-axis obtained by using ordinary state-based peridynamics.

For numerical discretization, a uniform discretization size of $\Delta x = 0.01\text{m}$ was utilized. The steady-state solution was obtained by utilizing Adaptive Dynamic Relaxation (ADR) (Madenci and Oterkus, 2014). The solution was first achieved by using ordinary state-based formulation. A horizon size of $\delta = 3\Delta x$ was selected. Variation of horizontal displacements along the central *x*-axis and vertical displacements along the central *y*-axis for three different horizon shapes; circle, irregular and square, are shown in Fig. 5. Peridynamic results were compared against finite element analysis results obtained from ANSYS, a commercially finite element software. Although PD results of all horizon shapes agree well with ANSYS results for the horizontal displacements, square horizon shape case could not capture accurate vertical displacement results.

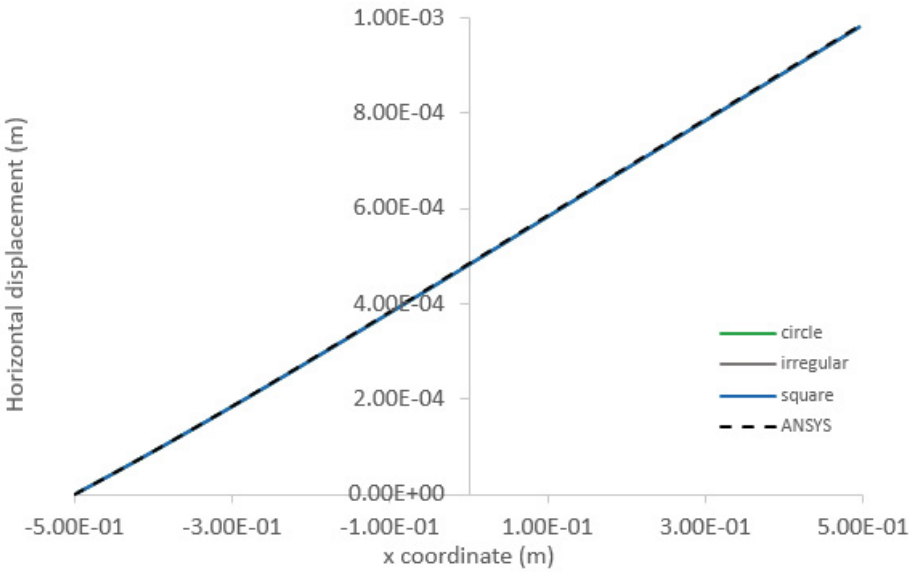

(a)

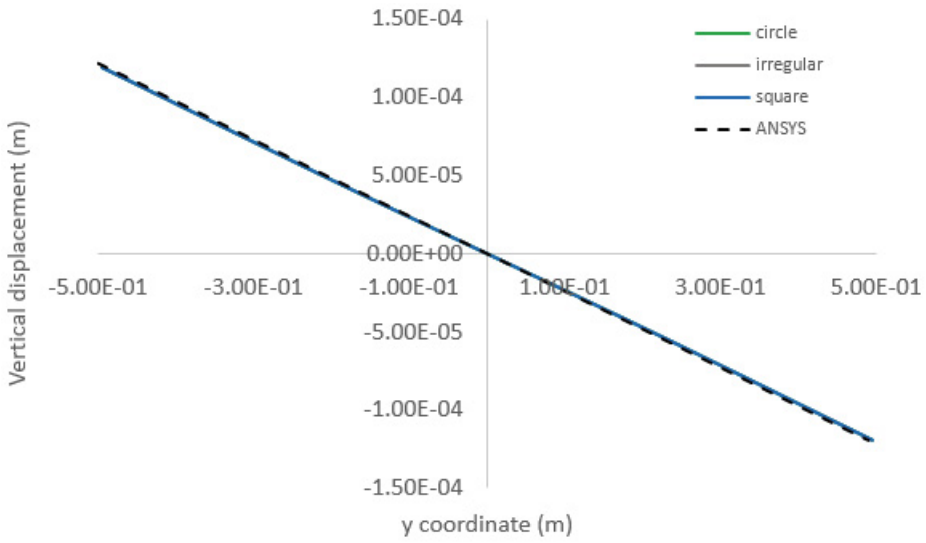

(b)

Fig. 6. Variation of **(a)** horizontal displacements along the central *x*-axis and **(b)** vertical displacements along the central y-axis obtained by using non-ordinary state-based peridynamics.

The same problem case was also analyzed by using non-ordinary state-based peridynamics. A horizon size of $\delta = 2\Delta x$ was selected. Variation of horizontal displacements along the central *x*-axis and vertical displacements along the central *y*-axis for three different horizon shapes are shown in Fig. 6. As opposed to ordinary state-based peridynamics results, for all three horizon shapes peridynamics results agree very well with ANSYS results for non-non-ordinary state-based peridynamics.

3.2. Vibration of a plate

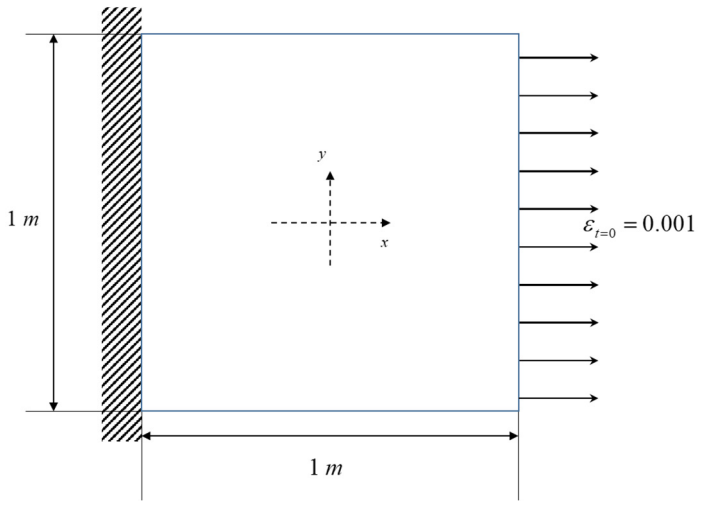

Fig. 7. Square plate subjected to initial uni-axial strain condition.

In the second problem case, the square plate subjected to initial uni-axial strain condition was considered as shown in Fig. 7. The square plate has a 1m edge length and thickness of 0.01 m. The elastic modulus, density and Poisson's ratio were specified as 200 GPa, 7850 kg/m^3 and 1/3, respectively. An initial uni-axial strain condition of $\varepsilon_{t=0} = 0.001$ in the *x*-direction was applied whereas the left edge is fully fixed.

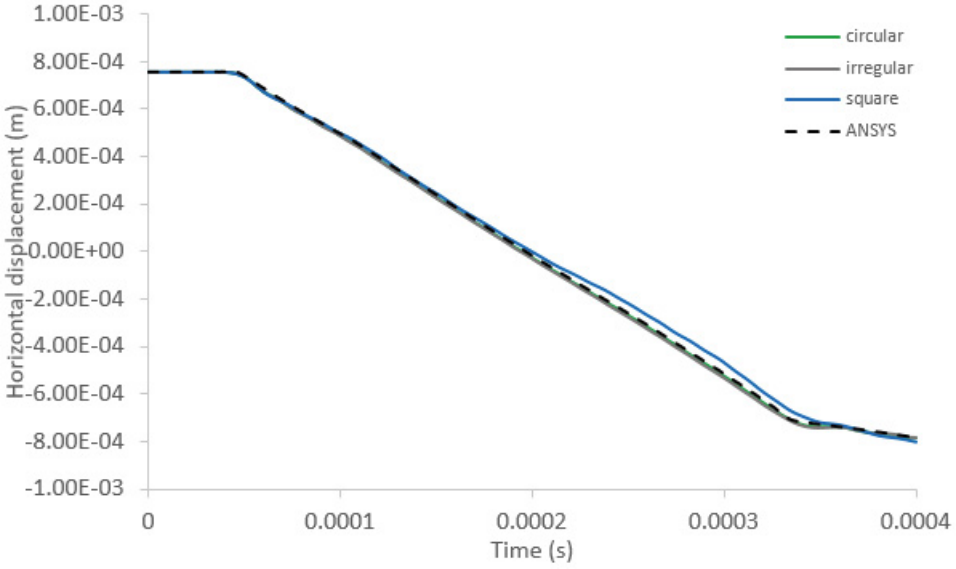

(a)

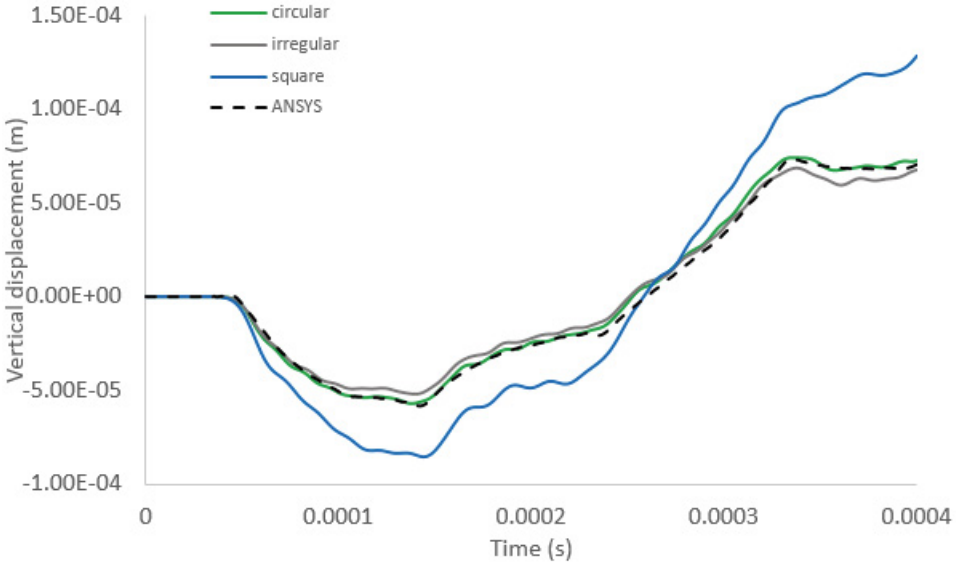

(b)

Fig. 8. Variation of **(a)** horizontal displacement and **(b)** vertical displacement of the material point located at (0.255 m, 0.255 m) with time obtained by using ordinary state-based peridynamics.

For numerical discretization, a uniform discretization size of $\Delta x = 0.01\,\text{m}$ was utilized. The dynamic solution was obtained by utilizing explicit time integration with a time step size of $\Delta t = 1\times10^{-7}\,\text{s}$. The solution was first achieved by using ordinary state-based formulation. A horizon size of $\delta = 3\Delta x$ was selected. Variation of horizontal and vertical displacements at a particular material point located at $(0.255\,\text{m}, 0.255\,\text{m})$ for the three different horizon shapes are shown in Fig. 8. Although PD results of all horizon shapes agree well with ANSYS results for the horizontal displacement, square horizon shape case could not capture accurate vertical displacement results.

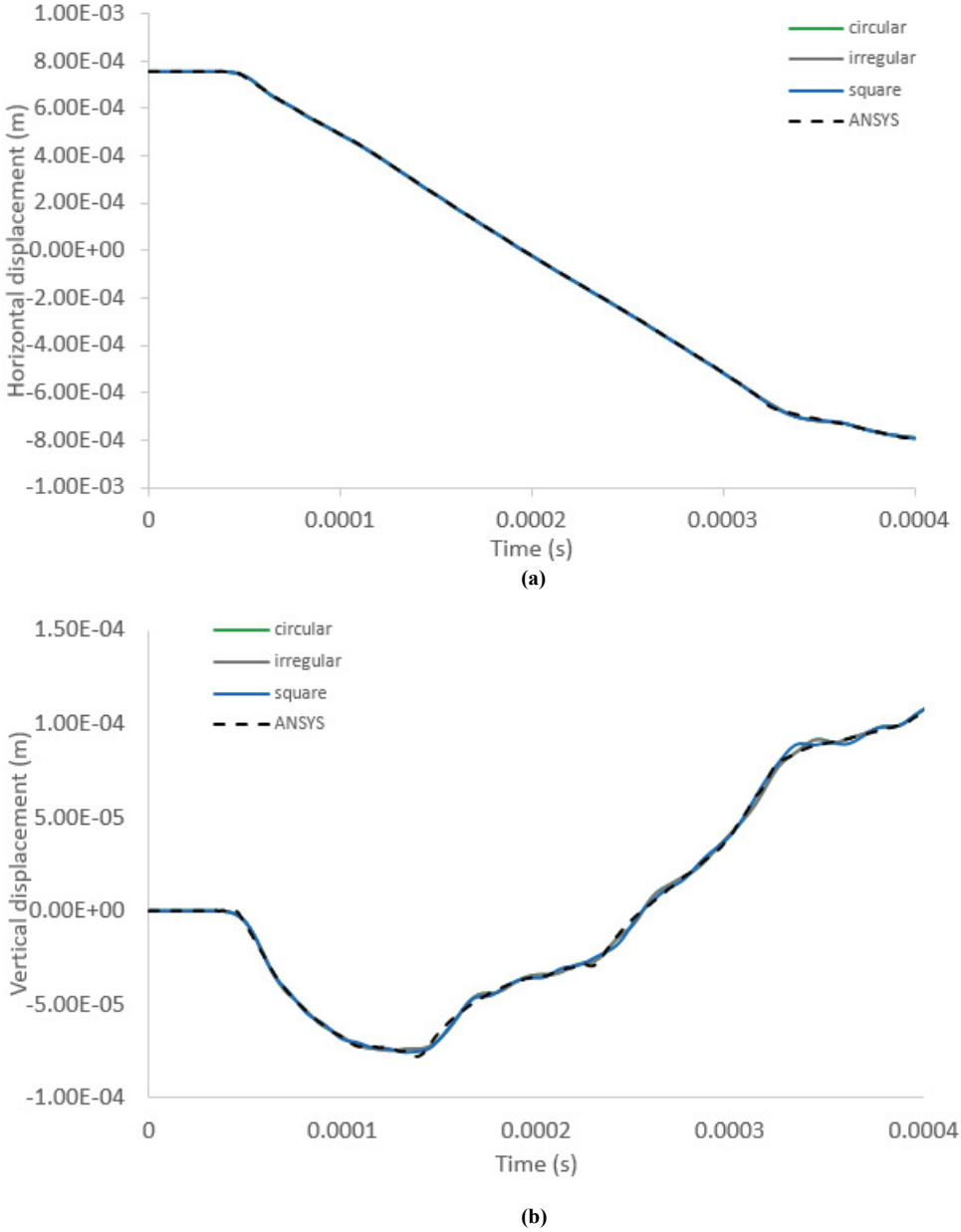

Fig. 9. Variation of **(a)** horizontal displacement and **(b)** vertical displacement of the material point located at (0.255 m, 0.255 m) with time obtained by using non-ordinary state-based peridynamics.

The same problem case was also analyzed by using non-ordinary state-based peridynamics. A horizon size of $\delta = 2\Delta x$ was selected. Variation of horizontal and vertical displacements at a particular material point located at $(0.255\,\mathrm{m}, 0.255\,\mathrm{m})$ for the three different horizon shapes are shown in Fig. 9. As opposed to ordinary state-based peridynamics results, for all three horizon shapes peridynamics results agree very well with ANSYS results for non-non-ordinary state-based peridynamics.

4. Conclusions

In this study, the effect of horizon shape was investigated for both ordinary state-based and non-ordinary state-based peridynamics. Three different horizon shapes were considered including circle, irregular and square. Both static and dynamic analyses were studied by considering plate under tension and vibration of a plate problems. For both static and dynamic conditions, square shape could not capture accurate vertical displacements for ordinary-state based peridynamics. On the other hand, results obtained for all three horizon shapes agreed very well with finite element analysis results for non-ordinary state-based peridynamics.

Acknowledgements

This material is based upon work supported by the Air Force Office of Scientific Research under award number FA9550-18-1-7004.

References

Basoglu, M.F., Zerin, Z., Kefal, A., Oterkus, E., 2019. A computational model of peridynamic theory for deflecting behavior of crack propagation with micro-cracks. Computational Materials Science 162, 33–46.

Bobaru, F., Hu, W., 2012. The meaning, selection, and use of the peridynamic horizon and its relation to crack branching in brittle materials. International journal of fracture 176(2), 215–222.

De Meo, D., Zhu, N., Oterkus, E., 2016. Peridynamic modeling of granular fracture in polycrystalline materials. Journal of Engineering Materials and Technology 138(4), 041008.

De Meo, D., Oterkus, E., 2017. Finite element implementation of a peridynamic pitting corrosion damage model. Ocean Engineering 135, 76–83.

De Meo, D., Russo, L., Oterkus, E., 2017. Modeling of the onset, propagation, and interaction of multiple cracks generated from corrosion pits by using peridynamics. Journal of Engineering Materials and Technology 139(4), 041001.

Diyaroglu, C., Oterkus, S., Oterkus, E., Madenci, E., 2017a. Peridynamic modeling of diffusion by using finite-element analysis. IEEE Transactions on Components, Packaging and Manufacturing Technology 7(11), 1823–1831.

Diyaroglu, C., Oterkus, S., Oterkus, E., Madenci, E., Han, S., Hwang, Y., 2017b. Peridynamic wetness approach for moisture concentration analysis in electronic packages. Microelectronics Reliability 70, 103–111.

Diyaroglu, C., Oterkus, E., Oterkus, S., 2019. An Euler–Bernoulli beam formulation in an ordinary state-based peridynamic framework. Mathematics and Mechanics of Solids 24(2), 361–376.

Imachi, M., Tanaka, S., Bui, T.Q., Oterkus, S., Oterkus, E., 2019. A computational approach based on ordinary state-based peridynamics with new transition bond for dynamic fracture analysis. Engineering Fracture Mechanics 206, 359–374.

Imachi, M., Tanaka, S., Ozdemir, M., Bui, T.Q., Oterkus, S., Oterkus, E., 2020. Dynamic crack arrest analysis by ordinary state-based peridynamics. International Journal of Fracture 221(2), pp.155–169.

Javili, A., Morasata, R., Oterkus, E., Oterkus, S., 2019. Peridynamics review. Mathematics and Mechanics of Solids 24(11), 3714-3739.

Kefal, A., Sohouli, A., Oterkus, E., Yildiz, M., Suleman, A., 2019. Topology optimization of cracked structures using peridynamics. Continuum Mechanics and Thermodynamics 31(6), 1645–1672.

Liu, X., He, X., Wang, J., Sun, L., Oterkus, E., 2018. An ordinary state-based peridynamic model for the fracture of zigzag graphene sheets. Proceedings of the Royal Society A: Mathematical, Physical and Engineering Sciences 474(2217), p.20180019.

Madenci, E., Oterkus, E., 2014. Peridynamic theory. Springer, New York, NY.

Oterkus, E., Barut, A., Madenci, E., 2010a. Damage growth prediction from loaded composite fastener holes by using peridynamic theory. In 51st AIAA/ASME/ASCE/AHS/ASC Structures, Structural Dynamics, and Materials Conference 18th AIAA/ASME/AHS Adaptive Structures Conference, Orlando, Florida, USA, p. 3026.

Oterkus, E., Guven, I. and Madenci, E., 2010b. Fatigue failure model with peridynamic theory. In 12th IEEE Intersociety Conference on Thermal and Thermomechanical Phenomena in Electronic Systems, Las Vegas, Nevada, USA, p. 1-6.

Oterkus, E., Madenci, E., 2012a. Peridynamics for failure prediction in composites. In 53rd AIAA/ASME/ASCE/AHS/ASC Structures, Structural Dynamics and Materials Conference 20th AIAA/ASME/AHS Adaptive Structures Conference, Honolulu, Hawaii, USA, p. 1692.

Oterkus, E., Madenci, E., 2012b. Peridynamic theory for damage initiation and growth in composite laminate. Key Engineering Materials 488, 355–358.

Oterkus, E., Guven, I., Madenci, E., 2012. Impact damage assessment by using peridynamic theory. Open Engineering 2(4), 523–531.

Oterkus, S., Madenci, E., Oterkus, E., Hwang, Y., Bae, J., Han, S., 2014, May. Hygro-thermo-mechanical analysis and failure prediction in electronic packages by using peridynamics. In 2014 IEEE 64th Electronic Components and Technology Conference (ECTC), Orlando, Florida, USA, p. 973-982.

Silling, S.A., 2000. Reformulation of elasticity theory for discontinuities and long-range forces. Journal of the Mechanics and Physics of Solids 48(1), 175–209.
Silling, S.A., Askari, E., 2005. A meshfree method based on the peridynamic model of solid mechanics. Computers & structures 83(17-18), 1526–1535.
Vazic, B., Wang, H., Diyaroglu, C., Oterkus, S., Oterkus, E., 2017. Dynamic propagation of a macrocrack interacting with parallel small cracks. AIMS Materials Science 4(1), pp.118–136.
Vazic, B., Oterkus, E., Oterkus, S., 2020. Peridynamic model for a Mindlin plate resting on a Winkler elastic foundation. Journal of Peridynamics and Nonlocal Modeling, pp.1–10.
Wang, H., Oterkus, E., Oterkus, S., 2018. Predicting fracture evolution during lithiation process using peridynamics. Engineering Fracture Mechanics 192, 176–191.
Wang, B., Oterkus, S., Oterkus, E., 2020. Determination of horizon size in state-based peridynamics. Continuum Mechanics and Thermodynamics, 1–24.
Yang, Z., Oterkus, E., Nguyen, C.T., Oterkus, S., 2019. Implementation of peridynamic beam and plate formulations in finite element framework. Continuum Mechanics and Thermodynamics 31(1), 301–315.
Yang, Z., Vazic, B., Diyaroglu, C., Oterkus, E., Oterkus, S., 2020. A Kirchhoff plate formulation in a state-based peridynamic framework. Mathematics and Mechanics of Solids 25(3), 727–738.
Zhu, N., De Meo, D., Oterkus, E., 2016. Modelling of granular fracture in polycrystalline materials using ordinary state-based peridynamics. Materials 9(12), p.977.